Original Article

MECHANICAL LOAD RESCUES INJURY-INDUCED SKELETAL MUSCLE FIBROSIS THROUGH MACROPHAGE POLARIZATION

H.W. Liu[1,2,§], S.G. Yuan[3,4,§], K. Zheng[3,4], G.F. Liu[1], Y. Xie[1], X.L. Huang[1], B.F. Ye[3,4], L. Yin[2,*], Y.K. Li[1,5,*] and J.H. Li[1,*]

[1]School of Traditional Chinese Medicine, Southern Medical University, 510000 Guangzhou, Guangdong, China
[2]Clinical Research Center, Department of Orthopaedic, Panzhihua Central Hospital, 617000 Panzhihua, Sichuan, China
[3]Department of Orthopaedic, Guangdong Provincial Hospital of Chinese Medicine, Hainan Hospital, Guangzhou University of Chinese Medicine, 570100 Haikou, Hainan, China
[4]Department of Orthopaedic, Hainan Traditional Chinese Medicine Hospital, Hainan Medical University, 570100 Haikou, Hainan, China
[5]Department of Traditional Chinese Orthopedics and Traumatology, Center for Orthopedic Surgery, The Third Affiliated Hospital, Southern Medical University, 510000 Guangzhou, Guangdong, China
[§]These authors contributed equally.

Abstract

Background: Current therapeutic approaches for skeletal muscle fibrosis are insufficient. We hypothesize that mechanical load (ML) could mitigate muscle fibrosis by suppressing inflammation. **Methods:** We utilized ML to treat cardiotoxin (CTX) injury-induced skeletal muscle fibrosis in C57BL6/J mice. We analyzed the underlying mechanism by integrating single-cell RNA sequencing (scRNA-seq) with molecular techniques. Hematoxylin and eosin staining and Masson's trichrome staining were used to assess skeletal muscle fibrosis. An enzyme-linked immunosorbent assay was used to detect inflammatory cytokine levels in serum. scRNA-seq, immunofluorescence, and Western blot were performed to determine cellular and molecular outcome changes. **Results:** After seven days of ML intervention, compared with CTX injury-induced fibrosis mice, ML significantly reduced pro-inflammatory cytokines interleukin (IL)-1β and IL-6 expression and increased anti-inflammatory cytokines transform growth factor (TGF)-β and IL-10 expression levels (all $p < 0.05$). Meanwhile, ML inhibited the expression of the fibrosis signaling pathway TGF-β1/Smad3 and decreased hyperplasia of fibrosis tissue in skeletal muscle (all $p < 0.05$). Next, scRNA-seq detected that M1 macrophage numbers, activity, and communication capacity are maximum increased in fibrotic skeletal muscle among B cells, endothelial cells, fast muscle cells, fibroblasts, skeletal muscle satellite cells, neutrophils, and T cells. However, ML significantly suppresses the expression of $CD68^+$ M1 macrophage and p65 in the nuclear factor kappa-B (NF-κB) pathway and promotes the $CD206^+$ M2 macrophage and peroxisome proliferator-activated receptor (PPAR)-γ expression levels in fibrotic skeletal muscle (all $p < 0.05$). **Conclusion:** ML can attenuate fibrosis in the injured skeletal muscle of mice by prompt polarization of M1 macrophages into M2 macrophages.

Keywords: Mechanical load, skeletal muscle fibrosis, macrophage, polarization, inflammation.

***Address for correspondence**: L. Yin, Clinical Research Center, Department of Orthopaedic, Panzhihua Central Hospital, 617000 Panzhihua, Sichuan, China. Email: yinli2913@163.com; Y.K. Li, School of Traditional Chinese Medicine, Southern Medical University, 510000 Guangzhou, Guangdong, China; Department of Traditional Chinese Orthopedics and Traumatology, Center for Orthopedic Surgery, The Third Affiliated Hospital, Southern Medical University, 510000 Guangzhou, Guangdong, China. Email: ortho@smu.edu.cn; J.H. Li, School of Traditional Chinese Medicine, Southern Medical University, 510000 Guangzhou, Guangdong, China. Email: lijunhua929@smu.edu.cn.

Introduction

Skeletal muscle fibrosis impedes muscular function and resilience, obstructing tissue regeneration following injury and enhancing re-injury likelihood (Mahdy, 2019). Fibrous tissue plays a pivotal role in force transmission and post-injury maintenance and repair of muscle fibers (Moyer and Wagner, 2011). However, excessive accumulation of fibrous tissue impairs muscle function and interferes with muscle fiber regeneration (Liu *et al*., 2024a). The fibrotic process is typically accompanied by a coordinated infiltration and activation of immune cells, which play a pivotal role in the clearance of damaged muscle fibers (Chazaud and Mounier, 2021; Sosa *et al*., 2021). These immune cells secrete a unique array of cytokines and growth factors that promote the activation and differentiation of satellite cells and guide the neighboring stromal cells in extracellular matrix (ECM) remodeling and angiogenesis (Kalaoja *et al*., 2021; Qualls *et al*., 2021; Wu *et al*., 2022). As such, immunomodulation has emerged as a potential strategy for mitigating skeletal muscle fibrosis, opening up new therapeutic avenues. Administration of immunomodulatory agents to the injury site has shown promise in preclinical studies (Millozzi *et al*., 2023; Van Damme *et al*., 2020). Certain materials currently in clinical use for muscle defect repair have been postulated to stimulate a pro-healing immune response. However, surgical interventions often risk severe complications and significant costs, highlighting an ongoing clinical need for a straightforward, economical, and non-invasive therapy for injury-induced skeletal muscle fibrosis.

Mechanical load (ML) encompasses various application methods, such as spinal manipulation, manual therapy, and mechanical compression. Spinal manipulation and manual therapy, also known as Tuina or massage in China, both involve the application of ML to tissues. This therapeutic approach has been traditionally used to alleviate pain, reduce inflammation, and enhance tissue repair (Yao *et al*., 2022). It is widely endorsed in alternative and complementary medicine for its capacity to facilitate musculoskeletal tissue rehabilitation (Aguilar-Agon *et al*., 2021; Bernard *et al*., 2022). This potential is likely to arise from many effects, including improved blood circulation, decreased oxidative stress, and augmented mitochondrial biogenesis (Barbe *et al*., 2021). Research focusing on muscle regeneration has demonstrated that ML can significantly modulate the inflammatory response within the tissue by attenuating inflammatory cytokine levels (Dziki *et al*., 2018; Loerakker *et al*., 2010). Despite these findings, the anti-inflammatory mechanisms of ML and its potential anti-fibrotic impact on skeletal muscle remain largely unexplored.

Our study aimed to ascertain whether ML can effectively mitigate the fibrosis induced by skeletal muscle injury, specifically through regulating macrophage polarization, thereby inhibiting the incidence and maintenance of muscle fibrosis. In our study, pro-inflammatory macrophages (M1) were screened as a critical cell cluster for ML in fibrosis relief. We demonstrated that ML can improve the inflammatory levels and anti-fibrosis in skeletal muscle by inhibiting the activation of the M1 macrophage and promoting polarization to anti-inflammatory macrophages (M2). Thus, our findings provide experimental and theoretical foundations for potential anti-fibrotic mechanisms of ML.

Fig. 1. Diagram of ML intervention. ML, mechanical load.

Materials and Methods

Study Design

Our investigation employed 24 male C57BL6/J mice weighing 20–25 g. In brief, the mice were subjected to an intramuscular injection of snake venom cardiotoxin (CTX) to induce a skeletal muscle fibrosis model following injury. Serum levels of pro-/anti- inflammatory factors and skeletal muscle histology were measured after seven days of ML treatment. Subsequently, we analyzed single-cell RNA sequencing (scRNA-seq) data from the Gene Expression Omnibus (GEO) database to identify the cell populations with the most significant changes during fibrosis after skeletal muscle injury. Finally, molecular and cellular outcome changes were determined.

Injury-Induced Skeletal Muscle Fibrosis Model and ML Treatment

Skeletal muscle fibrosis was induced in male C57BL6/J mice using an injection of CTX. This well-established model triggers fibrotic lesions in the skeletal muscle concurrent with muscle injury. It is valued as an experimental representation of skeletal muscle fibrosis due to the direct harm to muscle fibers, excluding defects in satellite or immune cells. Prior to CTX administration, the mice were anesthetized with 2 % isoflurane. The mice were randomized and allocated into four groups: normal (n = 6), sham (Phosphate Buffered Solution (PBS), n = 6), model (CTX, n = 6), and mechanical load (ML, n = 6). During anesthesia, a 10 μL injection of CTX (10 μg/mL) was administered into the right tibialis anterior

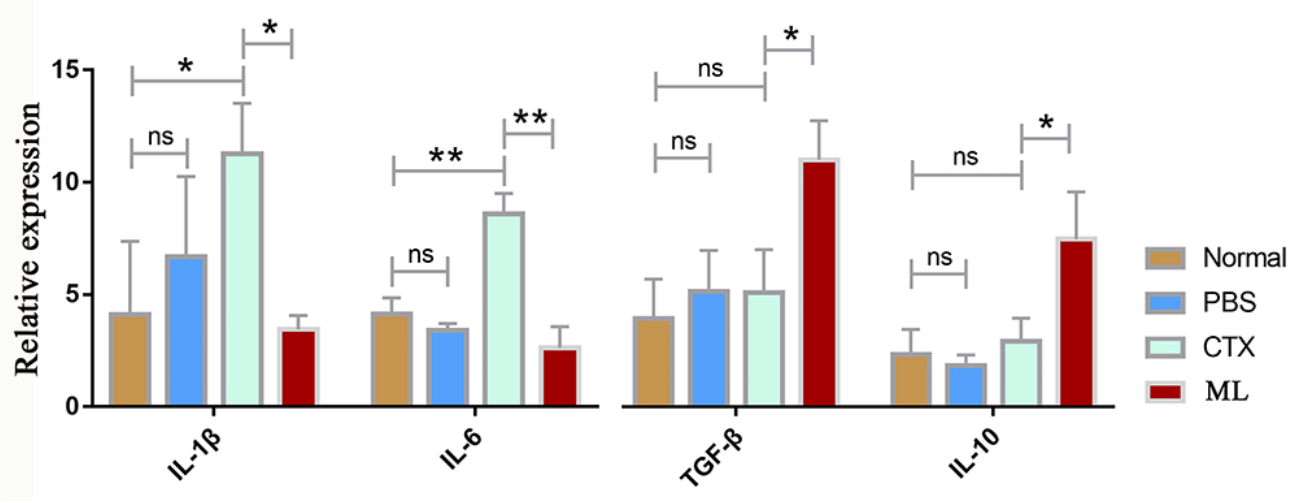

Fig. 2. IL-1β, IL-6, TGF-β, and IL-10 relative expression. IL, interleukin; TGF-β, transform growth factor beta; CTX, cardiotoxin; PBS, Phosphate Buffered Solution; ns, no significance. *$p < 0.05$, **$p < 0.01$. ns, $p > 0.05$.

Table 1. Cell numbers of each cluster.

Groups	B cells	Endothelial	Fast muscle	Fibroblasts	Macrophages	MuSCs	Neutrophils	T cells
CON	0	1055	99	1682	856	217	47	437
CTX	41	1881	488	1419	3477	277	875	486

MuSCs, muscle satellite cells.

(TA) muscle. The normal group received no treatment, whereas the sham group was injected with 10 μL of PBS into the same muscle.

The specific ML intervention, based on both published research and our previous studies, was implemented as follows (Cezar *et al*., 2016; Seo *et al*., 2021; Yao *et al*., 2022):

1. The intervention began 24 hours post-injury and lasted seven consecutive days, with 5-minute sessions every 10 to 12 hours.

2. Mice were acclimatized to the experimenter's handling 10 minutes before the intervention.

3. A pressure tester was employed to apply pressure and knead the midpoint of the right TA muscle, with the tester offering real-time feedback on pressure levels and allowing for operator-controlled adjustments of maximum pressure (Fig. 1).

4. The pressure tester maintained a constant stimulation pressure of 0.5 N and a frequency of 1 Hz.

Groups not receiving ML experienced daily handling, similar to the ML group, to control for potential stress effects. Following treatment, mice were returned to their cages. On day eight, the TA muscle and serum were isolated from the mice with and without ML.

Enzyme-Linked Immunosorbent Assay (ELISA)

Serum levels of interleukin (IL)-1β, IL-6, transform growth factor (TGF)-β, and IL-10 were measured using ELISA kits (Beyotime, Shanghai, China) according to the manufacturer's guidelines, with each sample analyzed in duplicate. Briefly, blood samples were collected from mice and allowed to clot for 30 minutes at room temperature. The samples were centrifuged at 2000 × g for 10 minutes to separate the serum. The serum was collected and stored at –80 °C until analysis. 96-well plates were coated with capture antibodies specific for IL-1β, IL-6, TGF-β, and IL-10 for the assay and incubated overnight at 4 °C. After washing, plates were blocked with a blocking buffer for 1 hour at room temperature. Serum samples and standards were added to the wells and incubated for 2 hours at room temperature. Plates were washed and incubated with detection antibodies for 1 hour, followed by a streptavidin-Horseradish Peroxidase (HRP) conjugate for 30 minutes. After a final wash, substrate solution was added, and the reaction was stopped with a stop solution. Absorbance was measured at 450 nm using a microplate reader, and cytokine concentrations were calculated based on standard curves.

Histological Analysis

On day eight, the TA muscle was extracted from mice to assess myofiber size and fibrosis degree. The TA muscle was harvested, fixed in 4 % paraformaldehyde, embedded in paraffin, and sectioned into 4 μm slices. These sections underwent heating at 60 °C for two hours, followed by dewaxing with xylene, gradual rehydration using alcohol, and rinsing with PBS. Eosin counterstaining was applied for 20 seconds, followed by rinsing in tap water. The slides were then immersed in 70 % ethanol for 1 minute, followed by 100 % ethanol for 1 minute, and

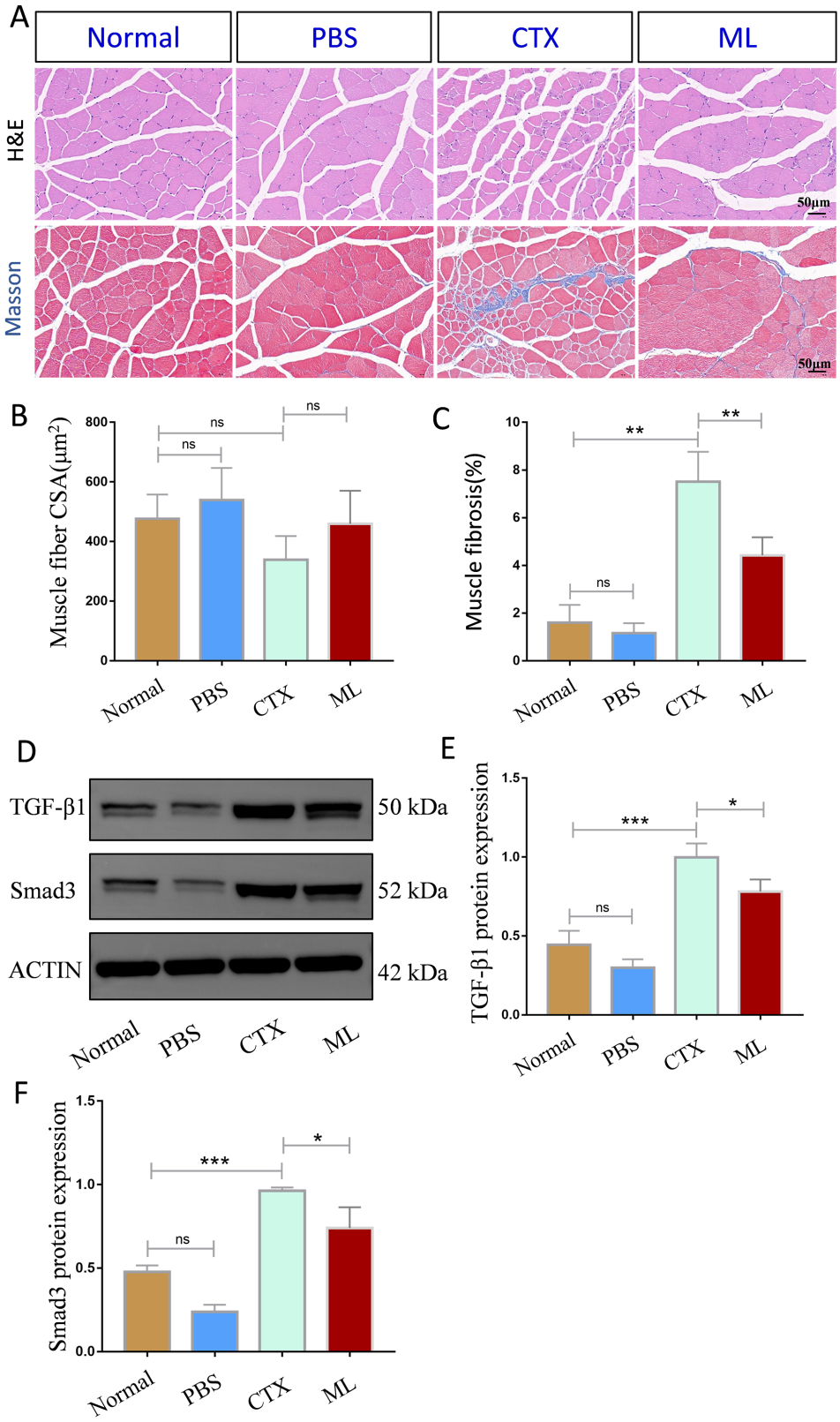

Fig. 3. MT treatment for muscle fibrosis. (**A**) Representative H&E and Masson's trichrome (collagen in blue) images of cross-histological sections of TA muscle. Scale bars = 50 μm. (**B**) Quantification of muscle fibers cross-sectional areas. (**C**) Percentage of fibrotic regions (appearing as blue in Masson's trichome in (A)). (**D–F**) Western blot analysis shows the relative protein expression of TGF-β1 and Smad3, respectively. ML, mechanical load; H&E, hematoxylin and eosin; TA, tibialis anterior; CSA, cross-sectional area. Scale bars = 50 μm. *$p < 0.05$, **$p < 0.01$, ***$p < 0.001$. ns, $p > 0.05$.

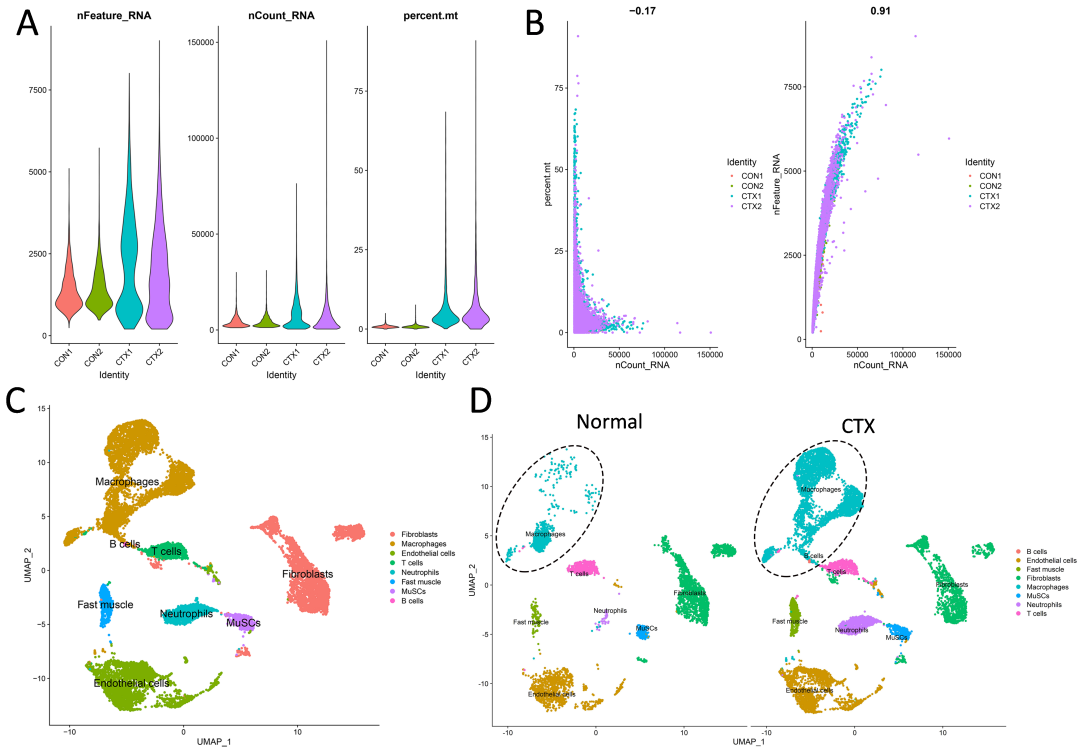

Fig. 4. Single-cell transcriptomic profiling of skeletal muscle fibrosis induced by injury. (**A**) The gene features, gene counts, and mitochondrial gene percentages for each sample. (**B**) Correlation analysis between gene expression and counts in individual samples. (**C**) UMAP visualization of all sequenced cells categorized by cell type, with different colors distinguishing each cell type. (**D**) UMAP projection comparing control (CON) and muscle fibrosis (CTX) groups, highlighting macrophages with ellipses, which show an increase in the CTX group. UMAP, uniform manifold approximation and projection; MuSCs, muscle satellite cells.

then xylene for 1 minute. After drying, coverslips were mounted using a xylene-based mounting medium. For Masson's trichrome staining, the sections were deparaffinized in xylene, rehydrated through graded ethanol, and stained with Bouin's solution. After washing, the sections were stained with Weigert's iron hematoxylin and Biebrich scarlet-acid fuchsin. Collagen was differentiated using phosphomolybdic-phosphotungstic acid and then stained with aniline blue. Sections were briefly rinsed, differentiated in acetic acid, dehydrated through ethanol, cleared in xylene, and mounted. The cross-sectional area (CSA) of muscle fibers was evaluated using hematoxylin and eosin staining, while the extent of fibrosis was quantified through Masson's trichrome staining with Image J software (version 1.80, National Institutes of Health, Bethesda, MD, USA). All histological analyses were conducted in a blinded fashion.

scRNA-seq Data Processing

Our experimental design incorporated scRNA-seq data from the GEO dataset involving CTX-induced TA muscle injury in C57BL6/J mice, designated as the experimental group. For the control group, scRNA-seq data from healthy C57BL6/J mice were used. Specifically, we chose GSM3614992 and GSM3614993 as the control (CON) group and GSM4831162 and GSM4831163 as the skeletal muscle injury group (CTX). Both groups were processed using 10X Genomics v2 chemistry with three-month-old mice. Each sample was derived from a single C57BL/6J mouse, and the material used was whole muscle cells from the TA. After sequencing, these data underwent scRNA-seq using the Illumina NovaSeq platform (Illumina HiSeq 3000, Illumina, San Diego, CA, USA) and were subsequently processed with the CellRanger software (version 7.2.0, 10X Genomics, Pleasanton, CA, USA) to generate the feature-barcode gene expression matrix. The Seurat R package (version 4.3.0) was utilized for downstream analyses, including principal component analysis (PCA) and uniform manifold approximation and projection (UMAP). We excluded cells containing fewer than 200 genes, more than 7500 genes, or more than 20 % mitochondrial genes. As a result, 13,337 filtered cells were included in the analysis. Significant principal components (PCs) were identified through PCA, and the *p*-value distribution was visualized using the JackStraw and ScoreJackStraw functions. A batch correction was performed with the "Harmony" R package (version 0.1.1) to address potential batch effects caused by sample identity, which could otherwise interfere with downstream analysis. We selected ten PCs for UMAP analysis. Cells were grouped into fourteen distinct clusters

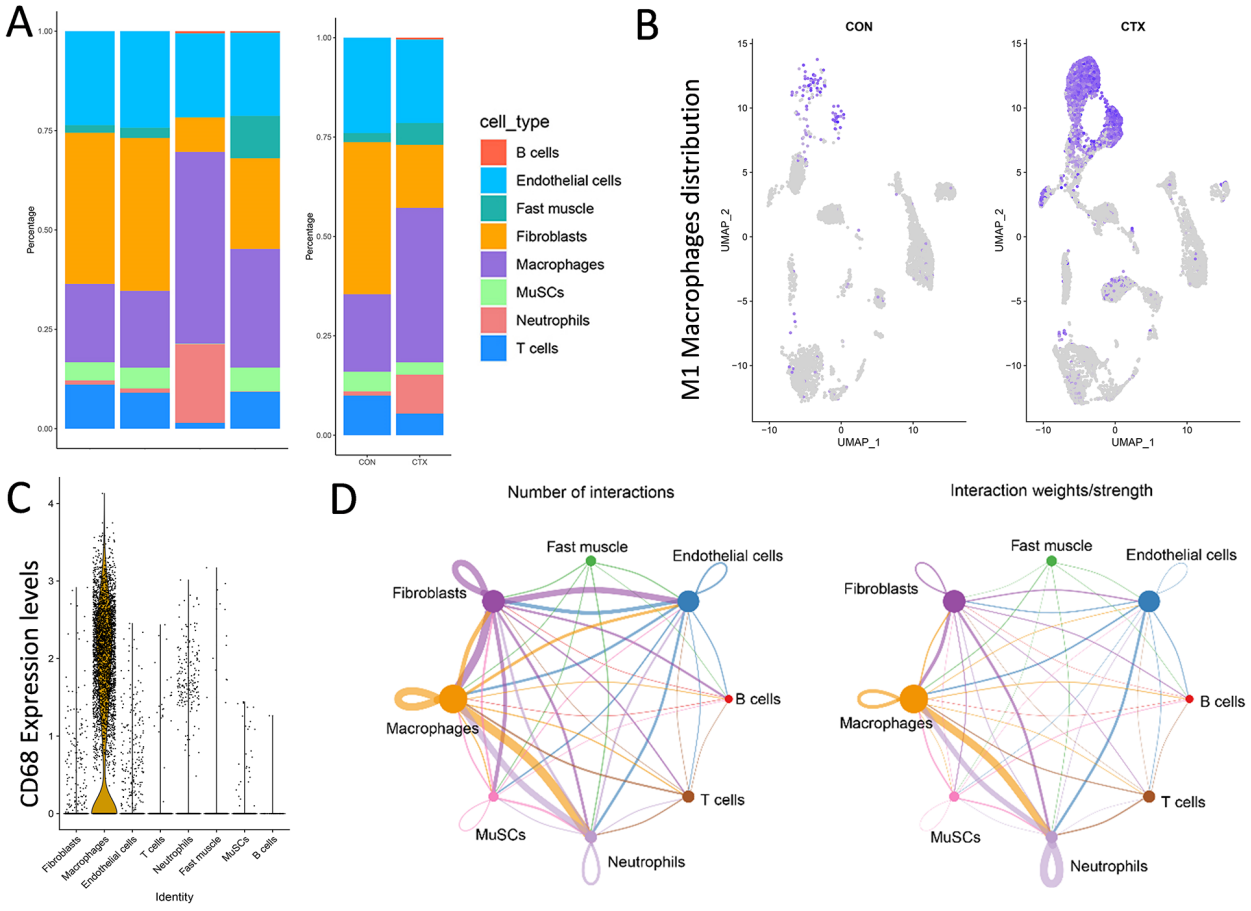

Fig. 5. Changes in cell clusters associated with injury-induced skeletal muscle fibrosis. (**A**) Distribution of clusters across each sample and group. (**B**) M1 macrophage distribution between the CON and CTX groups. (**C**) Expression levels of the M1 macrophage marker CD68 in various cell clusters. (**D**) Communication between cell clusters is displayed, with the left panel showing the total number of interactions and the right showing the interaction weights/strength. The dot size and line thickness represent the calculated communication strength.

at a resolution 0.5 using the FindClusters function. Differentially expressed genes (DEGs) for each cluster were identified with the FindAllMarkers function, applying a logfc.Threshold of 0.25. Cell types were determined based on the DEGs for each cluster and were cross-referenced with findings from a previous study (Liu *et al*., 2024b; Liu *et al*., 2024a).

Cell-Cell Communication and Correlation Analysis

To infer and evaluate cell-to-cell communication, we employed CellChat (version 1.6.0), a publicly available resource containing ligands, receptors, cofactors, and their interactions. Recognized for its flexibility and user-friendly interface, the CellChat toolkit, alongside the web-based Explorer (http://www.cellchat.org/), enables the discovery of novel intercellular communication pathways and the creation of comprehensive cell communication atlases. Concerning cell-interaction analysis, we gauged expression levels relative to the total read mapping to an identical set of coding genes across all transcriptomes. After that, expression values were averaged within each unique single-cell cluster or cell sample.

Immunofluorescence

As previous histological analysis outlined, TA muscle tissue slides were subjected to heating and deparaffinization. Following this, skeletal muscle sections were subjected to primary antibodies overnight at 4 °C to identify $CD68^+$ M1 macrophages (#ab53444, Abcam, Cambridge, UK) and $CD206^+$ M2 macrophages (#GB113497-100, Servicebio, Wuhan, China). After three washes in phosphatebuffered saline with Tween 20 (PBST), sections were treated with Cy3-labeled (#A0516, Beyotime Biotechnology, Shanghai, China) and Fluorescein Isothiocyanate (FITC)-labeled (#BA1101, BosterBio, Shanghai, China) secondary antibodies, respectively, for 60 minutes in darkness. The sections were then washed three times with PBST, followed by nuclear staining using 4′,6-diamidino-2-phenylindole (DAPI) (#1002, Beyotime Biotechnology, Shanghai, China) for 2 minutes. TA muscle tissue sections

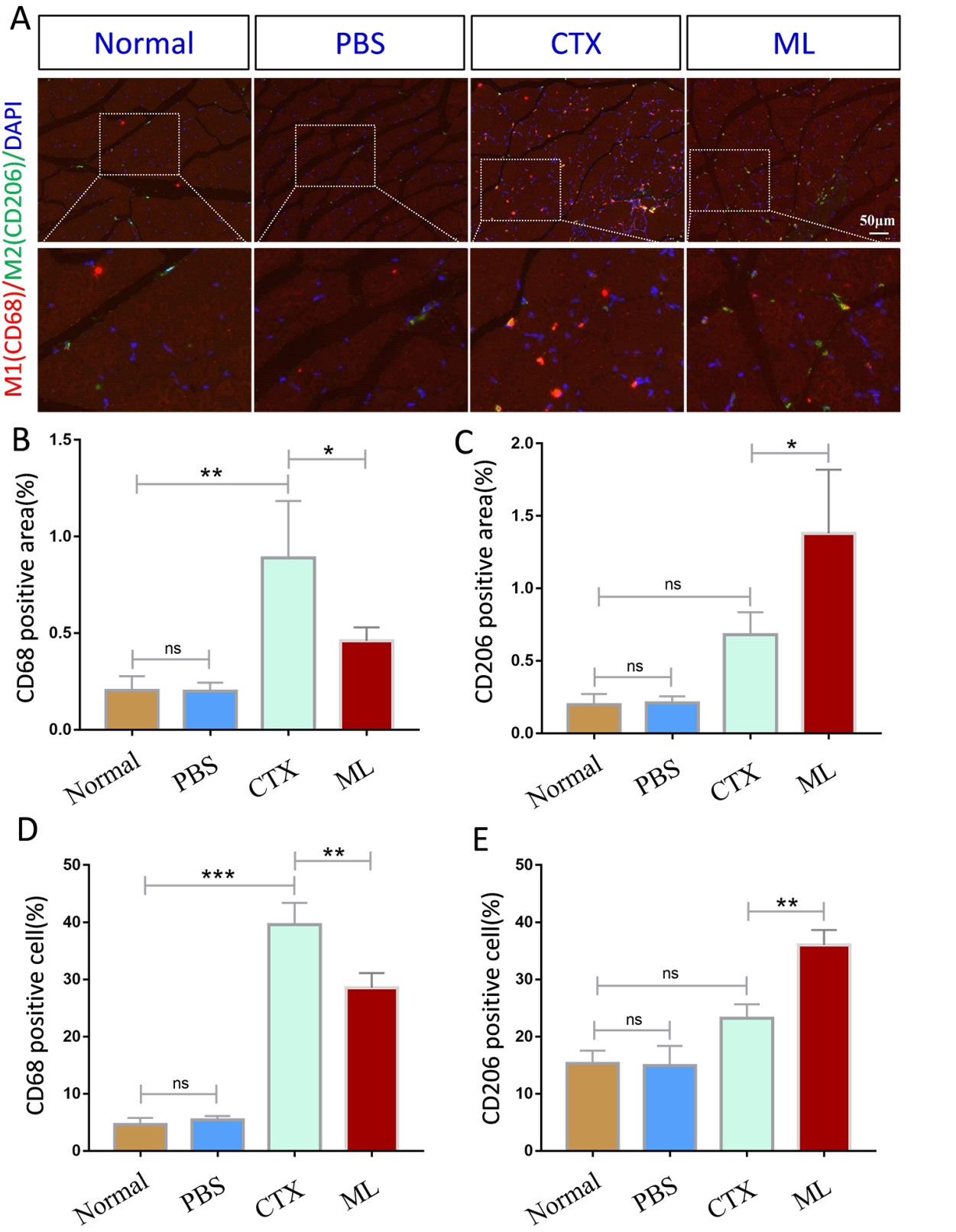

Fig. 6. Characterization of M1 macrophages and M2 macrophages. (**A**) Representative Immunofluorescence images of cross-sectional TA muscle tissue and nuclear staining were performed with DAPI (blue). (**B,C**) The proportion of CD68 and CD206 positive areas, shown in red and green, respectively, in the immunofluorescence images in (A). (**D,E**) The proportion of CD68 and CD206 positive cells compared to DAPI-stained nuclei. TA, tibialis anterior; DAPI, 4′,6-diamidino-2-phenylindole. Scale bars = 50 μm. *$p < 0.05$, **$p < 0.01$, ***$p < 0.001$. ns, $p > 0.05$.

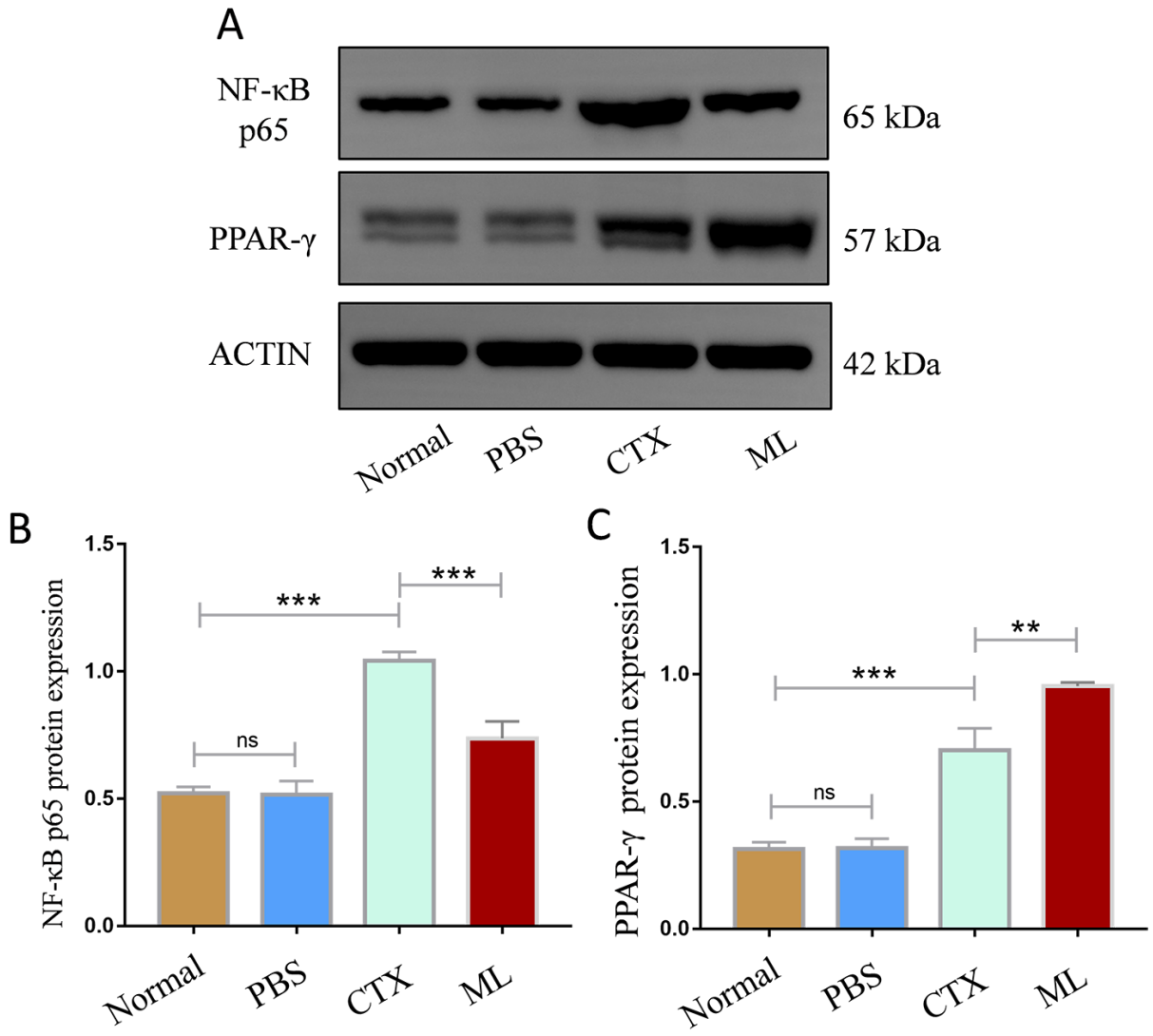

Fig. 7. Expression of macrophage polarization relative proteins. (**A**) Western blot illustrating the relative protein expression levels of (**B**) NF-κB p65 and (**C**) PPAR-γ. $^{**}p < 0.01$, $^{***}p < 0.001$. ns, $p > 0.05$; NF-κB, nuclear factor kappa-B; PPAR, peroxisome proliferator-activated receptor.

were imaged using a BX43 microscope (Olympus, Tokyo, Japan). For each section, three fields were randomly selected, and the average fluorescence intensity of the target protein was quantified using Image J software (version 1.80, National Institutes of Health, Bethesda, MD, USA).

Western Blot

Total protein was isolated from TA muscle tissue using radioimmunoprecipitation assay (RIPA) buffer. Protein concentration was determined using a bicinchoninic acid protein assay kit. Equal amounts of protein were separated by sodium dodecyl sulfate-polyacrylamide gel electrophoresis (SDS-PAGE) and transferred onto polyvinylidene fluoride membranes. Membranes were blocked with 5 % non-fat milk and incubated overnight at 4 °C with primary antibodies against TGF-β1 (1:500, #5154LF, CST, Boston, MA, USA), Smad3 (1:1000, #9523S, CST), nuclear factor kappa-B (NF-κB) p65 (1:1000, #GB11997, Servicebio, Wuhan, China), and peroxisome proliferator-activated receptor (PPAR)-γ (1:1000, #GB11164, Servicebio) in PBS. Following Tris-buffered saline with Tween 20 (TBST) washes, the membranes were incubated with secondary antibodies for 60 minutes at room temperature. Protein bands were detected using the ChemiDoc MP system (#1708280, Bio-Rad, Hercules, CA, USA) in combination with an enhanced chemiluminescence (ECL) kit (#E423-01, Vazyme, Nanjing, China). Band intensities were quantified using Image J software. All experiments were conducted in triplicate to ensure data reliability.

Statistical Analyses

Statistical analyses were performed using GraphPad Prism Software (version 7, San Diego, CA, USA), and the results were expressed as mean ± standard deviation. The Shapiro-Wilk test was used to assess the normality of the data. For data that followed a normal distribution, Student's *t*-tests were used for comparisons between two groups, and analysis of variance (ANOVA) was applied for comparisons among multiple groups. Post hoc pairwise comparisons after ANOVA were conducted using Tukey's test. For nonparametric or non-normally distributed data, Mann-Whitney U and Kruskal-Wallis tests were employed to compare two groups and multiple groups, respectively, with Dunn's test used for post hoc comparisons. Additionally, a two-way ANOVA with Bonferroni's post hoc test was used to evaluate data with two independent variables. Statistical significance was set at $p < 0.05$. The thresholds for establishing statistical significance were as follows: $*p < 0.05$, $**p < 0.01$, $***p < 0.001$.

Results

ML Attenuates M1 Macrophage-Derived Pro-Inflammatory Factors and Mitigates Skeletal Muscle Fibrosis

IL-1β and IL-6 are principal pro-inflammatory factors secreted by M1 macrophages, and TGF-β and IL-10 are anti-inflammatory factors secreted by M2 macrophages. ML involved applying a 0.5 N force and a frequency of 1 Hz, which began 24 hours post-injury and continued for seven days. The serum expression levels of IL-1β and IL-6 were substantially reduced, and TGF-β and IL-10 were increased (all $p < 0.05$) following ML treatment (Fig. 2). CTX injections led to skeletal muscle damage, instigating the high expression of pro-inflammatory factors IL-1β and IL-6 and escalating skeletal muscle fibrosis. However, skeletal muscle fibers showed no significant atrophy ($p > 0.05$). The CSA of muscle fibers, an indicator of muscle growth and contractile strength, does not demonstrate larger myofibers in the ML-treated muscle (Fig. 3**A,B**). Concurrently, applying the 0.5 N force resulted in a significant decrease (all $p < 0.05$) in interstitial fibrosis and the expression of TGF-β1 and Smad3 protein levels (Fig. 3**C–F**).

M1 Macrophage Numbers, Activity, and Communication Capacity are Increased in Fibrotic Skeletal Muscle

To elucidate the cell types undergoing the most significant changes during skeletal muscle fibrosis, we analyzed scRNA-seq data from skeletal muscle injury in C57BL6/J mice following CTX injection. We compared it with data from normal mice. scRNA-seq data from the GEO dataset were integrated to characterize the cell populations. Upon filtration, 8944 cells from injured (CTX) mice and 4393 cells from control (CON) subjects remained for analysis. The expression characteristics of each sample are depicted in Fig. 4**A**. A positive correlation was found between the number of unique molecular identifiers and the number of genes, with a correlation coefficient of 0.91 (Fig. 4**B**). Eight cell populations were identified and visualized using uniform manifold approximation and projection (UMAP) plots (Fig. 4**C**) based on cell type-specific marker genes. These included B cells ($CD19^+$, $MS4A1^+$, $CD22^+$), endothelial cells ($PECAM1^+$, $CD34^+$), fast muscle cells ($MYH1^+$), fibroblasts ($PDGFRA^+$), macrophages ($CSF1R^+$, $CD206^+$, $CD68^+$), skeletal muscle satellite cells (MuSCs: $Myod1^+$, $Pax7^+$), neutrophils ($S100a8^+$, $S100a9^+$, $CD14^+$, $ITGAM^+$), and T cells ($CD3D^+$, $CD3E^+$, $CD8A^+$).

Significant changes in cell clusters were detected within the macrophage, neutrophil, and fast muscle cell clusters. The macrophage cluster, highlighted by ellipses, showed an elevated percentage in the CTX group (Fig. 4**D**). Table 1 details the number of cells in each cluster. At the same time, Fig. 5**A** illustrates the proportions of cells across these clusters. Pro-inflammatory M1 macrophages predominated within the macrophage clusters, displaying notably increased numbers and activity (Fig. 5**B,C**). In addition to the macrophage cluster, the neutrophil and fast muscle clusters showed a notable increase in the CTX group compared to the CON group. Analysis of communication between the eight identified cell clusters revealed macrophages as the most active and communicative cells, dominating intercellular communication following skeletal muscle injury (Fig. 5**D**). These findings suggest that post-injury, M1 macrophages become the most numerous, active, and communicative cells, dominating the inflammation level and significantly impacting skeletal muscle capacity and function. Therefore, we hypothesize that M1 macrophages are key regulators of inflammation in skeletal muscles. In the following analyses, the primary focus was placed on M1 macrophages.

ML Promotes the Polarization of M1 Macrophages to M2 Macrophages

Macrophages play an essential role in skeletal muscle fibrosis after injury. M1 macrophages secrete pro-inflammatory factors, whereas M2 macrophages release anti-inflammatory factors. The effective recruitment and polarization of M1 and M2 macrophages are instrumental in restoring homeostasis of inflammatory levels following skeletal muscle injury. To explore the impact of ML on macrophages, we evaluated the efficiency of the M1 to M2 macrophage polarization in mice with skeletal muscle injuries post-ML involving a 0.5 N force. After seven days of treatment, ML significantly reduced the populations of $CD68^+$ M1 macrophages and increased the populations of $CD206^+$ M2 macrophages in the TA muscle tissue compared to the CTX group. Immunofluorescence imaging revealed a broad distribution of $CD68^+$ M1 macrophages in the inflammatory muscles of the untreated group. In contrast, in the ML-treated muscles, these macrophages

were confined to specific regions (Fig. 6**A**). The intensity of $CD68^+$ M1 macrophage expression was notably decreased ($p < 0.05$) in the ML group compared to the CTX group (Fig. 6**B**). Conversely, the expression of $CD206^+$ M2 macrophages exhibited the opposite trend, with significantly increased ($p < 0.05$) intensity in the ML group compared to the CTX group (Fig. 6**C**). Analysis of the percentage of CD68/$CD206^+$ cells confirmed (all $p < 0.05$) these trends (Fig. 6**D,E**). Consequently, NF-κB p65 protein expression levels in local muscle tissues were significantly reduced, while PPAR-γ protein expression levels were significantly elevated (all $p < 0.05$) in the ML group compared to the CTX group (Fig. 7**A–C**). This suggests that ML efficiently redirects pro-inflammatory M1 macrophages towards becoming anti-inflammatory M2 macrophages, thereby decreasing the expression levels of pro-inflammatory factors, such as IL-1β and IL-6, and alleviating the fibrosis induced by damaged skeletal muscle (**Supplementary file**).

Discussion

Skeletal muscle fibrosis, a prevalent consequence of muscular injuries, dystrophies, and aging, detrimentally impacts skeletal muscles' functional and structural aspects and hinders muscle fiber regeneration post-injury (Sosa *et al*., 2021). Importantly, it also escalates muscle susceptibility to recurrent injuries (Van Den Hoek *et al*., 2021). Our study presents compelling evidence for the potential nexus between ML and anti-fibrotic immune responses. Specifically, our findings highlight that: (1) macrophages are the most abundant and active immune cells, playing a predominant role in fibrotic skeletal muscle; (2) ML intervention can significantly reduce pro-inflammatory cytokines IL-1β and IL-6 expression and increase anti-inflammatory cytokines TGF-β and IL-10 expression levels; (3) ML inhibited the expression of the fibrosis signaling pathway TGF-β1/Smad3 and decreased hyperplasia of fibrosis tissue in skeletal muscle; (4) early application of ML can hinder the activation of M1 macrophages and promote their polarization into M2 macrophages. Thus, our findings provide experimental and theoretical foundations for potential anti-fibrotic mechanisms of ML. To the best of our knowledge, this study constitutes the first instance of empirical evidence suggesting that ML can mitigate the formation of fibrosis following skeletal muscle injury, which contributes novel insights towards the potential deployment of ML as a preventative strategy against muscle fibrosis.

ML via cyclic muscle tissue compression is a common strategy among athletes to alleviate skeletal muscle discomfort and expedite recovery following intense physical exertion (Seo *et al*., 2021). Skeletal muscle comprises various cell types capable of detecting and responding to mechanical stresses through a physiological process termed mechanotransduction. Emerging evidence underscores ML's immunomodulatory influence on skeletal muscle homeostasis. In the present investigation, we elucidated ML's ability to regulate the immune micro-environment status during skeletal muscle fibrosis following injury, mainly focusing on macrophage activity. A previous study also highlighted that applying cyclic compressive loading immediately after injury induced by eccentric exercise decreased the number of inflammatory macrophages and neutrophils within the muscle (Seo *et al*., 2021). However, this trend may be context-specific, as previous work observed load-dependent increases in macrophage populations within the healthy TA muscle of rats subjected to massage. Moreover, *in vitro* studies have shown that applying mechanical loading to a scaffold encourages macrophages to adopt an anti-inflammatory/restorative phenotype (Adams *et al*., 2019; Ji *et al*., 2020; Dziki *et al*., 2018). Interestingly, applying controlled cyclic compressive loading to uninjured muscle triggers the expression of genes associated with immune responses and the infiltration of $CD68^+$ and $CD163^+$ cells in a load-dependent manner.

Macrophages' quantity, activity, and communication capacity dictate the outcome—either muscle regeneration or fibrotic tissue formation following muscle injury (Chazaud, 2020). This study observed a significant post-injury increase in M1 macrophage numbers, activity, and communication capacity. Concurrently, the serum concentrations of IL-1β and IL-6 also significantly increased, aligning with previous findings. The phenomena of muscle fibrosis are intimately linked and concurrent with inflammation. Neutrophils are recruited to the injury site following muscle injury, facilitating the phagocytosis of damaged cells and initiating regeneration. Recruited neutrophils release chemoattractant cytokines, further promoting monocyte and macrophage infiltration. Immunomodulatory focuses on regulating the above processes and influencing the level of inflammation. Numerous studies have supported the immunomodulatory role of ML; however, previous work primarily focused on ML's effect on macrophage number, with minimal attention to macrophage polarization status (Seo *et al*., 2021; Cezar *et al*., 2016; Chazaud, 2020).

Macrophages, distinguished by two contrasting phenotypes, are pivotal in muscle fibrosis. The M1 phenotype, upon activation, releases pro-inflammatory cytokines, including IL-1β and IL-6, instigating the proliferation of fibroblasts (Panci and Chazaud, 2021; Shang *et al*., 2020). In contrast, the M2 phenotype produces TGF-β1 and fibronectin. An imbalance in the activation of M1 and M2 macrophages amplifies TGF-β1 expression. This amplified expression subsequently triggers resident fibroblast activation, forestalls fibro/adipogenic progenitors (FAPs) apoptosis, and provokes their differentiation into fibrogenic lineage (Torres-Ruiz *et al*., 2023). This cascade of events leads to the overaccumulation of the extracellular matrix (ECM) and, consequentially, fibrosis (Tidball and Villalta, 2010; Toumi *et al*., 2006). Our findings show that ML can encour-

age M1 macrophage polarization into M2 macrophages, thereby reducing the secretion of pro-inflammatory factors IL-1β and IL-6 and mitigating skeletal muscle fibrosis. *In vivo*, tissue compression is also suggested to modulate macrophage inflammatory status, decrease the adherence of pro-fibrotic macrophages, and expedite the removal of immune cells and metabolic waste products through enhanced fluid transportation (Chazaud, 2016; Tidball, 2002; Ziemkiewicz *et al*., 2021). Nonetheless, a recent investigation posits that the functional enhancements brought about by cyclic muscle tissue compression are not correlated with changes in macrophage count or inflammatory status (Seo *et al*., 2021; Shang *et al*., 2020; Tidball, 2017). Instead, these improvements are ascribed to the early removal of neutrophils. This clearance process culminates in a diminished expression of various cytokines, including MMP9 and CCL3 (Liu *et al*., 2024b). These cytokines impede the proliferation and foster the differentiation of skeletal muscle satellite cells under *in vitro* conditions. The current study noted a significant increase in macrophage and neutrophil numbers seven days post-skeletal muscle injury. Still, macrophages exhibited the most prominent rise in quantity, activity, and communication capacity, thus becoming the dominant cells within the immune cell population. This suggests that although macrophages and neutrophils contribute to the post-injury inflammatory state, macrophages assume a more dominant role.

It is well-established that the classical M1/M2 dichotomy does not fully reflect the complexity of macrophage phenotypes, particularly during skeletal muscle regeneration and fibrosis. A recent study demonstrated that markers traditionally used to define M1 and M2 macrophages may fail to characterize the full spectrum of macrophage subtypes involved in these processes (Coulis *et al*., 2023). Our study specifically looked for Galectin-3 (Gal3)-positive fibrotic macrophages in our scRNA-seq data. However, we did not detect a clear population of $Gal3^{+}$ macrophages. This may be due to the timing of our sample collection, which might have needed to align with the peak presence of these fibrotic macrophages. It is known that the dynamics of macrophage populations vary over time during the regeneration process, and sampling at different stages might yield different results (Tu and Li, 2023). This limitation emphasizes the importance of conducting longitudinal studies to capture the temporal dynamics of various macrophage populations, including fibrotic subtypes. Despite this, our findings still contribute to understanding macrophage heterogeneity, and further investigation will provide deeper insights into the roles of specific macrophage subtypes in muscle regeneration and fibrosis.

Our study acknowledges certain limitations. Firstly, the quantification and standardization of ML remain challenging in current research. Previous studies determined an effective range of loading force for ML interventions in mice to be between 0.15 N and 0.6 N; forces below 0.15 N showed no therapeutic impact, and forces above 0.6 N caused damage (Seo *et al*., 2021). Based on these findings and our prior research, we selected 0.5 N as the therapeutic loading force for ML. Nonetheless, the effects of additional mechanical parameters, such as loading frequency, application point, and number of cycles, warrant further investigation (Cezar *et al*., 2016). Secondly, although we employed a skeletal muscle fibrosis model induced by CTX injection, the need for additional studies using other clinically relevant fibrosis models, for instance, those resulting from type 2 diabetes, ischemic injury, and denervation, is clear to guide clinical translation better. Thirdly, while our study illustrated that ML could mitigate muscle fibrosis partly through the early polarization of macrophages, which reduces the secretion of pro-inflammatory factors, the mechanistic link underlying this polarization requires further elucidation. Moreover, we only assessed macrophage polarization at a single time point during skeletal muscle fibrosis. While this allowed us to observe distinct changes in M1 and M2 macrophages at a specific phase, it did not capture the dynamics of the M1-to-M2 transition, known to occur naturally during muscle fibrosis. The M1-M2 switch is a critical aspect of the fibrosis process, and longitudinal data encompassing multiple time points would offer a more in-depth understanding of the temporal dynamics of macrophage populations (Chazaud, 2020). Future studies should better focus on examining these dynamics across different phases of muscle fibrosis to elucidate the roles of M1 and M2 macrophages. In addition to the limitations previously discussed, another potential limitation of our study is the lack of functional assessments, such as gait analysis or measurements of muscle strength post-healing. These metrics could provide further insight into the functional recovery following mechanical loading but were outside the scope of the present study. Furthermore, the short duration of the study may limit the understanding of the long-term effects of mechanical loading on muscle fibrosis. Future studies should incorporate functional assessments and extended observation periods to gain a more comprehensive understanding of the therapeutic impact of mechanical loading.

When juxtaposed with drug- or biologic-based therapies typically investigated in anti-fibrosis treatments, ML presents a lower barrier to clinical translation. This advantage is attributed to ML's noninvasive character, personalized therapeutic delivery, and the reduced burden of regulatory compliance (Cezar *et al*., 2016; Yao *et al*., 2022). Noninvasive and biologic-free approaches may hold promise for patients dealing with chronic inflammation, such as those with idiopathic inflammatory myopathies, cancer-related cachexia, or age-related sarcopenia (Aguilar-Agon *et al*., 2021; Cezar *et al*., 2016). Given the limited effectiveness of immunosuppressive drugs in these cases, physical therapy presents itself as a viable alternative. Interactions, whether synergistic or antagonistic, may exist between ML-based

therapies and those based on biological agents, underscoring the potential efficacy of tailored combinatorial therapeutic strategies.

Conclusions

The findings of this study corroborate the potential of ML to mitigate fibrosis induced by damaged skeletal muscle, which is achieved by regulating macrophage polarization. These insights hold significant promise for clinical applications, particularly in improving therapeutic strategies for patients with skeletal muscle fibrosis. However, the mechanistic link between ML and macrophage polarization necessitates further investigation to elucidate its clinical implications fully.

List of Abbreviations

ML, mechanical load; CTX, cardiotoxin; scRNA-seq, single-cell RNA sequencing; TA, tibialis anterior; IL, interleukin; TGF, transform growth factor; CSA, cross-sectional area; PCA, principal component analysis; UMAP, uniform manifold approximation and projection; PCs, principal components; DEG, differentially expressed gene; ECM, extracellular matrix; FAP, fibro/adipogenic progenitor; ELISA, Enzyme-Linked Immunosorbent Assay; ANOVA, analysis of variance; Gal3, Galectin-3; NF-κB, nuclear factor kappa-B; PPAR, peroxisome proliferator-activated receptor; GEO, Gene Expression Omnibus; PBS, Phosphate Buffered Solution; ns, no significance; DAPI, 4′,6-diamidino-2-phenylindole; PBST, phosphatebuffered saline with Tween 20; FITC, Fluorescein Isothiocyanate; MuSCs, muscle satellite cells.

Availability of Data and Materials

Single-cell RNA-seq counts and raw data have been posted on Gene Expression Omnibus (https://www.ncbi.nlm.nih.gov/gds/, GSE126834 and GSE159500), and the other datasets used and/or analyzed during the current study are available from the corresponding author on reasonable request.

Author Contributions

YKL, LY, and JHL led the conception and design of the study. HWL, GFL, and SGY did the database search, screening, quality assessment, and data extraction. KZ and BFY designed the experiments and workflow. YX and XLH did the statistical analysis and interpreted the data. HWL and JHL wrote the paper. All authors read and approved the final manuscript. All authors agreed to be accountable for all aspects of the work in ensuring that questions related to the accuracy or integrity of any part of the work were appropriately investigated and resolved.

Ethics Approval and Consent to Participate

All procedures were approved by the Southern Medical University's Institutional Animal Care and Use Committee (Approval No. L2023063) and were conducted in accordance with the "Guide for the Care and Use of Laboratory Animals" published by the National Institutes of Health (NIH Publications No. 8023, revised 1978). All experimental procedures were conducted under the ARRIVE guidelines.

Acknowledgments

Not applicable.

Funding

This study was supported by the Guangdong Basic and Applied Basic Research Foundation (No. 2024A1515011263), the Health Commission of Sichuan Province Medical Science and Technology Program (No. 24WSXT002), the Sanming Project of Medicine in Shenzhen (No. SZZYSM202108013), the Hainan Provincial Natural Science Foundation of China (No. 823RC596), the Hainan Provincial Health Industry Research Project (No. 22A200106), and the National Natural Science Foundation of China (No. 82274669 and No.82360941).

Conflict of Interest

The authors declare that the content of this article was composed in the absence of any financial or personal relationships that might inappropriately influence this study.

Supplementary Material

Supplementary material associated with this article can be found, in the online version, at https://doi.org/10.22203/eCM.v048a08.

References

Adams S, Wuescher LM, Worth R, Yildirim-Ayan E (2019) Mechano-Immunomodulation: Mechanoresponsive Changes in Macrophage Activity and Polarization. Annals of Biomedical Engineering 47: 2213-2231. DOI: 10.1007/s10439-019-02302-4.

Aguilar-Agon KW, Capel AJ, Fleming JW, Player DJ, Martin NRW, Lewis MP (2021) Mechanical loading of tissue engineered skeletal muscle prevents dexamethasone induced myotube atrophy. Journal of Muscle Research and Cell Motility 42: 149-159. DOI: 10.1007/s10974-020-09589-0.

Barbe MF, Harris MY, Cruz GE, Amin M, Billett NM, Dorotan JT, Day EP, Kim SY, Bove GM (2021) Key indicators of repetitive overuse-induced neuromuscular inflammation and fibrosis are prevented by manual therapy in a rat model. BMC Musculoskeletal Disorders 22: 417. DOI: 10.1186/s12891-021-04270-0.

Bernard C, Zavoriti A, Pucelle Q, Chazaud B, Gondin

J (2022) Role of macrophages during skeletal muscle regeneration and hypertrophy-Implications for immunomodulatory strategies. Physiological Reports 10: e15480. DOI: 10.14814/phy2.15480.

Cezar CA, Roche ET, Vandenburgh HH, Duda GN, Walsh CJ, Mooney DJ (2016) Biologic-free mechanically induced muscle regeneration. Proceedings of the National Academy of Sciences of the United States of America 113: 1534-1539. DOI: 10.1073/pnas.1517517113.

Chazaud B (2016) Inflammation during skeletal muscle regeneration and tissue remodeling: application to exercise-induced muscle damage management. Immunology and Cell Biology 94: 140-145. DOI: 10.1038/icb.2015.97.

Chazaud B (2020) Inflammation and Skeletal Muscle Regeneration: Leave It to the Macrophages! Trends in Immunology 41: 481-492. DOI: 10.1016/j.it.2020.04.006.

Chazaud B, Mounier R (2021) Diabetes-induced skeletal muscle fibrosis: Fibro-adipogenic precursors at work. Cell Metabolism 33: 2095-2096. DOI: 10.1016/j.cmet.2021.10.009.

Coulis G, Jaime D, Guerrero-Juarez C, Kastenschmidt JM, Farahat PK, Nguyen Q, Pervolarakis N, McLinden K, Thurlow L, Movahedi S, Hughes BS, Duarte J, Sorn A, Montoya E, Mozaffar I, Dragan M, Othy S, Joshi T, Hans CP, Kimonis V, MacLean AL, Nie Q, Wallace LM, Harper SQ, Mozaffar T, Hogarth MW, Bhattacharya S, Jaiswal JK, Golann DR, Su Q, Kessenbrock K, Stec M, Spencer MJ, Zamudio JR, Villalta SA (2023) Single-cell and spatial transcriptomics identify a macrophage population associated with skeletal muscle fibrosis. Science Advances 9: eadd9984. DOI: 10.1126/sciadv.add9984.

Dziki JL, Giglio RM, Sicari BM, Wang DS, Gandhi RM, Londono R, Dearth CL, Badylak SF (2018) The Effect of Mechanical Loading Upon Extracellular Matrix Bioscaffold-Mediated Skeletal Muscle Remodeling. Tissue Engineering. Part A 24: 34-46. DOI: 10.1089/ten.tea.2017.0011.

Ji X, Yuan X, Ma L, Bi B, Zhu H, Lei Z, Liu W, Pu H, Jiang J, Jiang X, Zhang Y, Xiao J (2020) Mesenchymal stem cell-loaded thermosensitive hydroxypropyl chitin hydrogel combined with a three-dimensional-printed poly(ε-caprolactone) /nano-hydroxyapatite scaffold to repair bone defects via osteogenesis, angiogenesis and immunomodulation. Theranostics 10: 725-740. DOI: 10.7150/thno.39167.

Kalaoja M, Corbin LJ, Tan VY, Ahola-Olli AV, Havulinna AS, Santalahti K, Pitkänen N, Lehtimäki T, Lyytikäinen LP, Raitoharju E, Seppälä I, Kähönen M, Ripatti S, Palotie A, Perola M, Viikari JS, Jalkanen S, Maksimow M, Salomaa V, Salmi M, Raitakari OT, Kettunen J, Timpson NJ (2021) The Role of Inflammatory Cytokines as Intermediates in the Pathway from Increased Adiposity to Disease. Obesity 29: 428-437. DOI: 10.1002/oby.23060.

Liu H, Yuan S, Liu G, Li J, Zheng K, Zhang Z, Zheng S, Yin L, Li Y (2024a) Satellite Cell-Derived Exosomes: A Novel Approach to Alleviate Skeletal Muscle Atrophy and Fibrosis. Advanced Biology 8: 2300558. DOI: 10.1002/adbi.202300558.

Liu H, Yuan S, Zheng K, Liu G, Li J, Ye B, Yin L, Li Y (2024b) IL-17 signaling pathway: A potential therapeutic target for reducing skeletal muscle inflammation. Cytokine 181: 156691. DOI: 10.1016/j.cyto.2024.156691.

Loerakker S, Stekelenburg A, Strijkers GJ, Rijpkema JJM, Baaijens FPT, Bader DL, Nicolay K, Oomens CWJ (2010) Temporal Effects of Mechanical Loading on Deformation-Induced Damage in Skeletal Muscle Tissue. Annals of Biomedical Engineering 38: 2577-2587. DOI: 10.1007/s10439-010-0002-x.

Mahdy MAA (2019) Skeletal muscle fibrosis: an overview. Cell and Tissue Research 375: 575-588. DOI: 10.1007/s00441-018-2955-2.

Millozzi F, Papait A, Bouché M, Parolini O, Palacios D (2023) Nano-Immunomodulation: A New Strategy for Skeletal Muscle Diseases and Aging? International Journal of Molecular Sciences 24: 1175. DOI: 10.3390/ijms24021175.

Moyer AL, Wagner KR (2011) Regeneration versus fibrosis in skeletal muscle. Current Opinion in Rheumatology 23: 568-573. DOI: 10.1097/BOR.0b013e32834bac92.

Panci G, Chazaud B (2021) Inflammation during post-injury skeletal muscle regeneration. Seminars in Cell & Developmental Biology 119: 32-38. DOI: 10.1016/j.semcdb.2021.05.031.

Qualls AE, Southern WM, Call JA (2021) Mitochondria-cytokine crosstalk following skeletal muscle injury and disuse: a mini-review. American Journal of Physiology. Cell Physiology 320: C681-C688. DOI: 10.1152/ajpcell.00462.2020.

Seo BR, Payne CJ, McNamara SL, Freedman BR, Kwee BJ, Nam S, de Lázaro I, Darnell M, Alvarez JT, Dellacherie MO, Vandenburgh HH, Walsh CJ, Mooney DJ (2021) Skeletal muscle regeneration with robotic actuation-mediated clearance of neutrophils. Science Translational Medicine 13: eabe8868. DOI: 10.1126/scitranslmed.abe8868.

Shang M, Cappellesso F, Amorim R, Serneels J, Virga F, Eelen G, Carobbio S, Rincon MY, Maechler P, De Bock K, Ho PC, Sandri M, Ghesquière B, Carmeliet P, Di Matteo M, Berardi E, Mazzone M (2020) Macrophage-derived glutamine boosts satellite cells and muscle regeneration. Nature 587: 626-631. DOI: 10.1038/s41586-020-2857-9.

Sosa P, Alcalde-Estévez E, Asenjo-Bueno A, Plaza P, Carrillo-López N, Olmos G, López-Ongil S, Ruiz-Torres MP (2021) Aging-related hyperphosphatemia impairs myogenic differentiation and enhances fibrosis in skeletal muscle. Journal of Cachexia, Sarcopenia and Muscle 12: 1266-1279. DOI: 10.1002/jcsm.12750.

Tidball JG (2002) Interactions Between Muscle and the Immune System During Modified Musculoskeletal Loading. Clinical Orthopaedics and Related Research 403:

S100-S109. DOI: 10.1097/00003086-200210001-00012.

Tidball JG (2017) Regulation of muscle growth and regeneration by the immune system. Nature Reviews. Immunology 17: 165-178. DOI: 10.1038/nri.2016.150.

Tidball JG, Villalta SA (2010) Regulatory interactions between muscle and the immune system during muscle regeneration. American Journal of Physiology. Regulatory, Integrative and Comparative Physiology 298: R1173-R1187. DOI: 10.1152/ajpregu.00735.2009.

Torres-Ruiz J, Alcalá-Carmona B, Alejandre-Aguilar R, Gómez-Martín D (2023) Inflammatory myopathies and beyond: The dual role of neutrophils in muscle damage and regeneration. Frontiers in Immunology 14: 1113214. DOI: 10.3389/fimmu.2023.1113214.

Toumi H, F'guyer S, Best TM (2006) The role of neutrophils in injury and repair following muscle stretch. Journal of Anatomy 208: 459-470. DOI: 10.1111/j.1469-7580.2006.00543.x.

Tu H, Li YL (2023) Inflammation balance in skeletal muscle damage and repair. Frontiers in Immunology 14: 1133355. DOI: 10.3389/fimmu.2023.1133355.

Van Damme N, Van Hecke A, Remue E, Van Den Bussche K, Moore Z, Gefen A, Verhaeghe S, Beeckman D (2020) Physiological processes of inflammation and edema initiated by sustained mechanical loading in subcutaneous tissues: A scoping review. Wound Repair and Regeneration: Official Publication of the Wound Healing Society [and] the European Tissue Repair Society 28: 242-265. DOI: 10.1111/wrr.12777.

Van Den Hoek AM, De Jong JCBC, Worms N, Van Nieuwkoop A, Voskuilen M, Menke AL, Lek S, Caspers MPM, Verschuren L, Kleemann R (2021) Diet and exercise reduce pre-existing NASH and fibrosis and have additional beneficial effects on the vasculature, adipose tissue and skeletal muscle via organ-crosstalk. Metabolism: Clinical and Experimental 124: 154873. DOI: 10.1016/j.metabol.2021.154873.

Wu Y, Wu Y, Yang Y, Yu J, Wu J, Liao Z, Guo A, Sun Y, Zhao Y, Chen J, Xiao Q (2022) Lysyl oxidase-like 2 inhibitor rescues D-galactose-induced skeletal muscle fibrosis. Aging Cell 21: e13659. DOI: 10.1111/acel.13659.

Yao C, Ren J, Huang R, Tang C, Cheng Y, Lv Z, Kong L, Fang S, Tao J, Fu Y, Zhu Q, Fang M (2022) Transcriptome profiling of microRNAs reveals potential mechanisms of manual therapy alleviating neuropathic pain through microRNA-547-3p-mediated Map4k4/NF-κb signaling pathway. Journal of Neuroinflammation 19: 211. DOI: 10.1186/s12974-022-02568-x.

Ziemkiewicz N, Hilliard G, Pullen NA, Garg K (2021) The Role of Innate and Adaptive Immune Cells in Skeletal Muscle Regeneration. International Journal of Molecular Sciences 22: 3265. DOI: 10.3390/ijms22063265.

Editor's note: The Scientific Editor responsible for this paper was Juerg Gasser.